Odd-Parity Magnons in the Haldane-Hubbard Model from Topological Exciton Condensation

Rintaro Eto* and Johannes Knolle

Technical University of Munich, TUM School of Natural Sciences, Physics Department, 85748 Garching, Germany and Munich Center for Quantum Science and Technology (MCQST), Schellingstraße 4, 80799 München, Germany

(Received 15 June 2026; accepted 16 October 2026; published 19 November 2026)

Collective excitations in condensed matter can carry nontrivial topology and provide information about quantum phases beyond their ground-state properties. At the same time, the recent emergence of altermagnetism and related nonrelativistic spin-split electronic states raises the question of how unconventional magnetic symmetry is encoded in their collective excitations. Here, we uncover a continuous evolution from topological excitons to odd-parity magnons across an interaction-driven magnetic transition in the paradigmatic Haldane-Hubbard model. In the paramagnetic phase, our newly found sharp topological excitons soften and condense into a collinear Néel state, where they evolve into Goldstone magnons displaying characteristic f-wave spin splitting. The topology of these collective modes is tied to the underlying electronic topology, such that an electron bandgap closing enforces a magnon bandgap closing, changing the magnon topology. Our results establish a direct connection between topological collective excitations and nonrelativistic odd-parity spin splittings, with potential realizations in Floquet-driven materials and cold atomic gases.

DOI: 10.1103/q1cs-j5py

Much of our understanding of quantum matter has been built around ground state properties, with symmetry breaking and topology providing powerful organizing principles for their classification. By comparison, the properties of excited states have received less systematic attention. This perspective is now changing as collective excitations such as excitons [1–5], magnons [6], and phonons [7] are increasingly recognized to possess nontrivial quantum topological properties of their own. Understanding how such excited-state properties relate to the underlying quantum phase and evolve across phase transitions is therefore becoming an important frontier.

A paradigmatic setting for addressing these questions is the Haldane-Hubbard (HH) model. The Haldane model [8] laid the foundation for modern topological band theory [9,10], while its interacting extension has become a minimal platform for correlated topological matter [11–13]. Extensive studies have established a rich ground-state phase diagram [14–22], including paramagnetic and collinear Néel phases with nontrivial electronic topology, yet the collective excitations remain basically unexplored. The HH model therefore offers a natural opportunity to ask how the topology of its well-established electronic and ground-state phases is reflected in the structure of its excitations and evolves across phases.

This question has acquired a new dimension with the recent conceptual establishment of altermagnetism [23–25], which has renewed broad interest in nonrelativistic momentum-dependent spin splitting in compensated magnets. Beyond even-parity altermagnets, odd-parity magnets have emerged as another class of nonrelativistic spin-split magnetic states [26–32]. Remarkably, the collinear Néel state of the HH model itself was recently recognized as an odd-parity magnet: its complex next-nearest-neighbor hoppings encode time-reversal-symmetry-breaking loop current order that, together with Néel order, generates an f-wave spin splitting of the electronic bands without spin-orbit coupling [33–35]. While the collective excitations of even-parity altermagnets have begun to be actively explored [36–41], those of odd-parity magnets [42,43] remain largely unknown. The HH model thus brings together two emerging questions: the topology of collective excitations and the manifestation of nonrelativistic odd-parity spin splitting beyond electronic bands.

In this Letter, we uncover that these two aspects of the HH model are intimately tied to each other. Across a symmetry-breaking transition, a topological collective mode can continuously change its quasiparticle character and associated spin-crystallographic symmetry while retaining its connection to the underlying electronic topology. In the paramagnetic phase, we identify sharp topological excitons whose condensation drives the

*Contact author: rintaro.eto@tum.de

Published by the American Physical Society under the terms of the Creative Commons Attribution 4.0 International license. Further distribution of this work must maintain attribution to the author(s) and the published article's title, journal citation, and DOI.

transition into the collinear Néel state. Upon the onset of magnetic order, the corresponding collective modes continuously evolve into Goldstone magnons that exhibit nonrelativistic f-wave spin splitting while retaining a topology tied to the underlying electronic bands. Consequently, an electronic topological transition enforces a magnon bandgap closing and changes the magnon topology. Our results establish a continuous link between topological excitons, odd-parity spin splitting, and topological magnons, revealing how topology and unconventional magnetism are encoded across the collective excitation spectrum.

Model—The Hamiltonian of the HH model on the two-dimensional honeycomb lattice is given by

$$\begin{aligned}\mathcal{H} = &-t_1 \sum_{\langle \mathbf{r},\mathbf{r}'\rangle_{\mathrm{NN}}} \sum_{\sigma=\uparrow,\downarrow} (\hat{c}^\dagger_{\mathbf{r}\sigma}\hat{c}_{\mathbf{r}'\sigma} + \mathrm{H.c.}) \\ &- t_2 \sum_{\langle \mathbf{r},\mathbf{r}'\rangle_{\mathrm{NNN}}} \sum_{\sigma=\uparrow,\downarrow} (e^{i\nu_{\mathbf{r},\mathbf{r}'}\phi}\hat{c}^\dagger_{\mathbf{r}\sigma}\hat{c}_{\mathbf{r}'\sigma} + \mathrm{H.c.}) \\ &+ U\sum_{\mathbf{r}} \hat{n}_{\mathbf{r}\uparrow}\hat{n}_{\mathbf{r}\downarrow}, \end{aligned} \tag{1}$$

where $\hat{c}^\dagger_{\mathbf{r}\sigma}$ ($\hat{c}_{\mathbf{r}\sigma}$) denotes an electron creation (annihilation) operator with spin σ at site $\mathbf{r}$. $\hat{n}_{\mathbf{r}\sigma} = \hat{c}^\dagger_{\mathbf{r}\sigma}\hat{c}_{\mathbf{r}\sigma}$ is the number operator. The first two terms correspond to the Haldane model, i.e., the nearest-neighbor (NN) and the next-nearest-neighbor (NNN) electron hopping on the honeycomb lattice, respectively. Note that t_1, $t_2 \geq 0$. The bond-dependent factor $\nu_{r,r'} = \pm 1$ sets the orientation of the complex NNN hoppings and the associated loop currents, as depicted in Fig. 1(a). We set $\phi = \pi/2$ throughout this work, for which the NNN hopping is purely imaginary and the time-reversal-breaking Haldane mass is maximal at fixed t_2. Such purely imaginary NNN hoppings also arise naturally in Floquet realizations of the Haldane model based on honeycomb lattices driven with circularly polarized light [44]. The third term is the onsite Hubbard repulsion. We consider the half-filled case and mainly discuss the intermediate interaction regime $U/t_1 = 4$. Before studying the dynamical properties of the HH model, we revisit its Hartree-Fock (HF) phase diagram originally presented about a decade ago [14]; see Fig. 1(c). When $t_2/t_1 \lesssim 0.4$, the system exhibits three distinct phases: (A) a topological paramagnetic phase in which the electron bands have nontrivial Chern numbers of $C_{v\uparrow} = C_{v\downarrow} = -C_{c\uparrow} = -C_{c\downarrow} = +1$, (B) a topological collinear antiferromagnetic (AFM) phase with $C_{v\uparrow} = C_{v\downarrow} = -C_{c\uparrow} = -C_{c\downarrow} = +1$, and (C) a nontopological collinear AFM phase; c and v are unoccupied and occupied band indices, respectively.

Time-dependent Hartree-Fock—Throughout this Letter, we study particle-hole excitations in the HH model using the time-dependent Hartree-Fock (TDHF) approximation [45–50]. In TDHF, exciton eigenmodes are obtained with the eigenvalue problem [51]

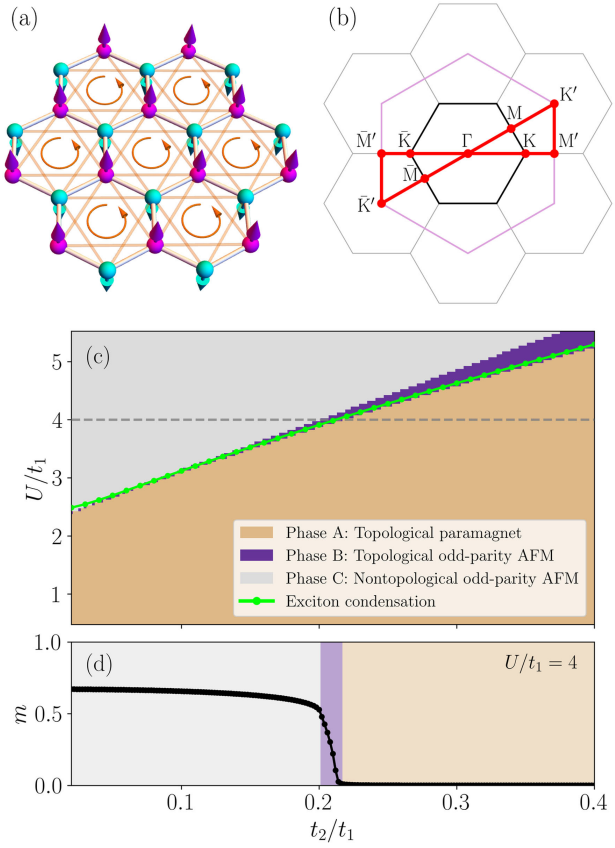


FIG. 1. (a) Schematic of the odd-parity magnetism in the Haldane-Hubbard (HH) model. Bravais vectors are given by $\mathbf{a}_1 = (1,0)$, $\mathbf{a}_2 = (-1/2, \sqrt{3}/2)$, and $\mathbf{a}_3 = (-1/2, -\sqrt{3}/2)$. Magenta and cyan arrows represent the collinear Néel order. Orange bonds and arrows denote loop currents encoded by imaginary hoppings. (b) Brillouin zones (BZs) of the Haldane-Hubbard model. Black, gray, and magenta hexagons represent the first, second, and extended BZs, respectively. Red lines and markers describe a certain momentum path and high-symmetry points referred in this work. (c) Hartree-Fock phase diagram of the HH model (color map), overlapped by paramagnetic-magnetic phase boundary (green line with markers) obtained with the time-dependent Hartree-Fock approximation. The gray dashed line denotes the cut at $U/t_1 = 4$, along which the dynamical spin structure factors shown in Figs. 2 and 4 are evaluated. (d) Magnitude of the mean-field Néel order parameter m (= sublattice magnetization $|\langle \sigma_z \rangle| = 2|\langle s_z \rangle|$) at fixed $U/t_1 = 4$ and varying t_2/t_1. The background colors indicate the phases A, B, and C, respectively.

$$\{[\mathcal{H}, Q^\dagger_{\mathbf{q},\nu,\sigma\to\bar{\sigma}}] - \hbar\omega_{\mathbf{q},\nu} Q^\dagger_{\mathbf{q},\nu,\sigma\to\bar{\sigma}}\}|0\rangle = 0, \tag{2}$$

where the creation operator of an exciton as a spin-flip ($\sigma \to \bar{\sigma}$) particle-hole pair in the Bogoliubov-de-Gennes (BdG) form $Q^\dagger_{\mathbf{q},\nu,\sigma\to\bar{\sigma}}$ is given by

$$\begin{aligned} Q^\dagger_{\mathbf{q},\nu,\sigma\to\bar{\sigma}} = \sum_{\mathbf{k}} \{ & X^{\sigma\to\bar{\sigma}}_{\mathbf{q},\nu}[\mathbf{k} - (1-\alpha)\mathbf{q}]\hat{c}^\dagger_{\mathbf{k}+\alpha\mathbf{q},c\bar{\sigma}}\hat{c}_{\mathbf{k}-(1-\alpha)\mathbf{q},v\sigma} \\ & - Y^{\sigma\to\bar{\sigma}}_{\mathbf{q},\nu}[\mathbf{k} - (1-\alpha)\mathbf{q}]\hat{c}^\dagger_{-\mathbf{k}+(1-\alpha)\mathbf{q},v\bar{\sigma}}\hat{c}_{-\mathbf{k}-\alpha\mathbf{q},c\sigma}\}, \end{aligned} \tag{3}$$

where $X^{\sigma\to\bar{\sigma}}_{\mathbf{q},\nu}[\mathbf{k}-(1-\alpha)\mathbf{q}]$ and $Y^{\sigma\to\bar{\sigma}}_{\mathbf{q},\nu}[\mathbf{k}-(1-\alpha)\mathbf{q}]$ are the envelope functions of excitons. Note that ν is an index of exciton bands. $|0\rangle$ denotes the correlated ground state. Different choices of Berry connection correspond to different conventions for assigning a collective position coordinate to the particle-hole excitation. These conventions can be parameterized by $\alpha\in[0,1]$ [3,52,53]. We confirmed that $\alpha=0$ and $\alpha=1$ yield identical results up to negligible numerical error [51]. We therefore present the results with $\alpha=1$ hereafter.

For finite size systems with a periodic boundary condition, the TDHF calculation for the downward spin-flip ($\uparrow\to\downarrow$) sector of the HH model is essentially given by the following paraunitary eigenvalue problem [51,54]:

$$\sum_{\mathbf{k}}\begin{pmatrix} A^{\uparrow\to\downarrow}_{\mathbf{q}}(\mathbf{k}',\mathbf{k}) & B^{\uparrow\to\downarrow}_{\mathbf{q}}(\mathbf{k}',\mathbf{k}) \\ \bar{B}^{\uparrow\to\downarrow}_{\mathbf{q}}(\mathbf{k}',\mathbf{k}) & \bar{A}^{\uparrow\to\downarrow}_{\mathbf{q}}(\mathbf{k}',\mathbf{k}) \end{pmatrix}\begin{pmatrix} X^{\uparrow\to\downarrow}_{\mathbf{q},\nu}(\mathbf{k}) \\ Y^{\uparrow\to\downarrow}_{\mathbf{q},\nu}(\mathbf{k}) \end{pmatrix} = \omega_{\mathbf{q},+-}\begin{pmatrix} 1 & 0 \\ 0 & -1 \end{pmatrix}\begin{pmatrix} X^{\uparrow\to\downarrow}_{\mathbf{q},\nu}(\mathbf{k}') \\ Y^{\uparrow\to\downarrow}_{\mathbf{q},\nu}(\mathbf{k}') \end{pmatrix}, \tag{4}$$

where

$$A^{\uparrow\to\downarrow}_{\mathbf{q}}(\mathbf{k}',\mathbf{k}) = (\varepsilon_{\mathbf{k}+\mathbf{q},c\downarrow}-\varepsilon_{\mathbf{k},v\uparrow})\delta_{\mathbf{k},\mathbf{k}'} - \frac{U}{N}\sum_{\alpha}\langle\mathbf{k},v|\sigma^{+}_{\alpha}|\mathbf{k}+\mathbf{q},c\rangle\langle\mathbf{k}'+\mathbf{q},c|\sigma^{-}_{\alpha}|\mathbf{k}',v\rangle, \tag{5}$$

$$B^{\uparrow\to\downarrow}_{\mathbf{q}}(\mathbf{k}',\mathbf{k}) = +\frac{U}{N}\sum_{\alpha}\langle-\mathbf{k}-\mathbf{q},c|\sigma^{+}_{\alpha}|-\mathbf{k},v\rangle\langle\mathbf{k}'+\mathbf{q},c|\sigma^{-}_{\alpha}|\mathbf{k}',v\rangle, \tag{6}$$

$$\bar{B}^{\uparrow\to\downarrow}_{\mathbf{q}}(\mathbf{k}',\mathbf{k}) = +\frac{U}{N}\sum_{\alpha}\langle\mathbf{k},v|\sigma^{+}_{\alpha}|\mathbf{k}+\mathbf{q},c\rangle\langle-\mathbf{k}',v|\sigma^{-}_{\alpha}|-\mathbf{k}'-\mathbf{q},c\rangle, \tag{7}$$

and

$$\bar{A}^{\uparrow\to\downarrow}_{\mathbf{q}}(\mathbf{k}',\mathbf{k}) = (\varepsilon_{-\mathbf{k}-\mathbf{q},c\uparrow}-\varepsilon_{-\mathbf{k},v\downarrow})\delta_{\mathbf{k},\mathbf{k}'} - \frac{U}{N}\sum_{\alpha}\langle-\mathbf{k}-\mathbf{q},c|\sigma^{+}_{\alpha}|-\mathbf{k},v\rangle \times\langle-\mathbf{k}',v|\sigma^{-}_{\alpha}|-\mathbf{k}'-\mathbf{q},c\rangle. \tag{8}$$

$\sigma^{\pm}_{\alpha}=(1/2)(\sigma^{x}_{\alpha}\pm i\sigma^{y}_{\alpha})$ denote the Pauli spin-flip operators acting on the sublattice-$\alpha(=\mathrm{A},\mathrm{B})$ basis. $|\mathbf{k},\nu\rangle$ is a Bloch state obtained within the self-consistent Hartree-Fock approximation [see End Matter] with momentum $\mathbf{k}$ and a band index ν. We consider system sizes up to 30^2 unit cells and find that finite size effects seen in the dispersion relation are negligibly small. We solve the paraunitary eigenvalue problem using Cholesky decomposition followed by a usual unitary diagonalization [55]. Chern numbers of the lowest exciton modes in each sector are calculated using the Wilson loop method [51,56] respecting D_6 symmetric distribution of the $\mathbf{k}$-mesh.

A key advantage of TDHF is that it provides a unified description of collective excitations across the excitonic condensation transition. Within the same formalism, excitons in the paramagnetic phase continuously evolve into magnons in the magnetically ordered phase, enabling a direct characterization of the change in quasiparticle nature associated with symmetry breaking [54,57].

Topological excitons—First, we focus on the paramagnetic phase. Figure 2(a) shows the dynamical spin-structure factor $S(\mathbf{q},\omega)$ obtained with the RPA [see End Matter for details] overlaid with the TDHF exciton bands $\{\omega_{\mathbf{q},\nu}\}$ along the high-symmetry momentum path defined in Fig. 1(b). Both RPA and TDHF show the existence of sharp low-energy modes, i.e., excitons. The doubly degenerate lowest exciton bands with mutually decoupled opposite spin-flip processes $\nu=+-(\uparrow\to\downarrow)$ and $\nu=-+(\downarrow\to\uparrow)$ are isolated from the upper particle-hole continuum by a tiny gap at the M point, and each possesses a Chern number of $C^{\uparrow\to\downarrow(\downarrow\to\uparrow)}_{\mathrm{exc}}=-2$. The exciton Chern number can be understood to originate from the difference in Chern numbers between unoccupied and occupied electron bands [58], i.e.,

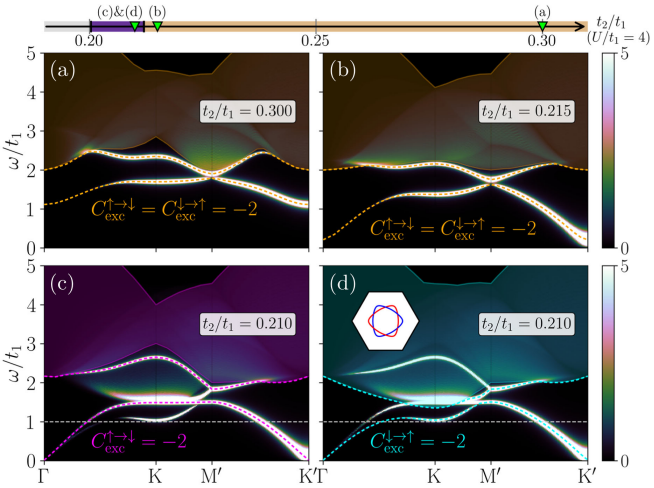


FIG. 2. (a),(b) Dynamical spin structure factor $S(\mathbf{q},\omega)=S_{+-}(\mathbf{q},\omega)+S_{-+}(\mathbf{q},\omega)$ of the HH model, overlaid with the TDHF spectra in the topological paramagnetic phase A. Colored dashed lines and shaded regions represent isolated collective modes and particle-hole continua, respectively. (c),(d) Same as (a),(b) but for the topological odd-parity AFM phase B, together with the spin-resolved TDHF spectra. Inset [in (d)]: the isoenergy contour of the TDHF spectrum at $\omega/t_1=1$, corresponding to the white dashed lines in (c) and (d). For all panels, $U/t_1=4$ and $\phi=\pi/2$. The values of t_2/t_1 are indicated in each panel and marked in the phase diagram at the top. Light gray, purple, and orange bands in the phase diagram show phases C, B, and A, respectively.

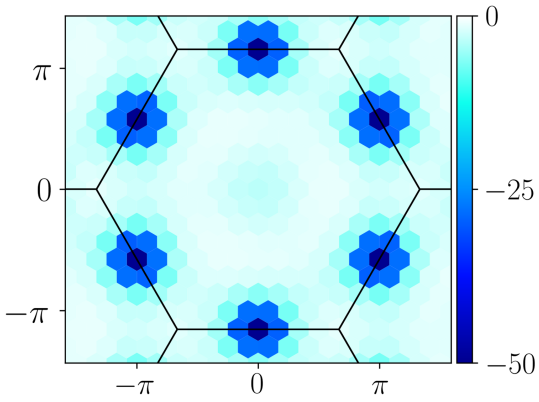


FIG. 3. Exciton Berry curvature of the lowest bands with $C_{\mathrm{exc}}^{\uparrow\to\downarrow(\downarrow\to\uparrow)}=-2$ in the paramagnetic phase A at $t_2/t_1=0.3$, $U/t_1=4$, and $\phi=\pi/2$. Note that the Berry curvature distribution is identical for $+-$ $(\uparrow\to\downarrow)$ and $-+$ $(\downarrow\to\uparrow)$ excitons. The black hexagon denotes the first Brillouin zone.

$$C_{\mathrm{exc}}^{\sigma\to\bar{\sigma}}=C_{c\bar{\sigma}}-C_{v\sigma}. \tag{9}$$

Thus, we have revealed sharp topological excitons as novel collective excitations already at intermediate interaction strength in the paradigmatic HH model.

Figure 3 shows the Berry curvature (BC) distribution of the lowest exciton band, which is identical for the upward and downward spin-flip sectors, $\uparrow\to\downarrow$ and $\downarrow\to\uparrow$. Sharp BC peaks appear at each of the three inequivalent M points, where the gap between the lowest exciton band and the upper continuum is minimal [see Fig. 2(a)]. This exciton BC distribution is in stark contrast to that of the underlying electron bands, whose nontrivial topology originates from bandgap closing and reopening at the K and $\bar{\mathrm{K}}$ points and is therefore accompanied by BC accumulation around them. Remarkably, despite the simple relation $C_{\mathrm{exc}}^{\sigma\to\bar{\sigma}}=C_{c\bar{\sigma}}-C_{v\sigma}$, the exciton BC is concentrated near the M points rather than the K and $\bar{\mathrm{K}}$ points that govern the electronic topology. This observation highlights that the momentum-space structure of exciton topology is not trivially inherited from that of the constituent electron and hole bands, but is instead strongly influenced by the collective nature of the particle-hole bound state. Notably, the exciton BC remains finite even near the optically accessible Γ point owing to broken time-reversal symmetry. This finite long-wavelength BC can generate an anomalous transverse velocity of exciton wave packets under an external potential or strain gradient, potentially leading to an exciton Hall drift.

Exciton topology is sometimes led by underlying crystalline symmetries [59]. It is noteworthy that the nontrivial exciton Chern number $C_{\mathrm{exc}}^{\uparrow\to\downarrow(\downarrow\to\uparrow)}=\pm 2 \bmod 6$ here can be understood from recently proposed stable exciton wave function (EWF) zeros [60]. We extend this concept to BdG systems, in which the EWF intensity is given by

$$\mathsf{m}_{\mathbf{q},\nu}^{\sigma\to\bar{\sigma}}(\mathbf{k})=|X_{\mathbf{q},\nu}^{\sigma\to\bar{\sigma}}(\mathbf{k})|^2-|Y_{\mathbf{q},\nu}^{\sigma\to\bar{\sigma}}(\mathbf{k})|^2. \tag{10}$$

In the topological paramagnetic phase of the HH model, it is numerically found that $\mathsf{m}_{\mathbf{q}=\Gamma,\nu=\mathrm{lowest}}^{\sigma\to\bar{\sigma}}(\mathrm{K})=\mathsf{m}_{\mathbf{q}=\Gamma,\nu=\mathrm{lowest}}^{\sigma\to\bar{\sigma}}(\bar{\mathrm{K}})=0$ and $\mathsf{m}_{\mathbf{q}=\Gamma,\nu=\mathrm{lowest}}^{\sigma\to\bar{\sigma}}(\mathbf{k})\neq 0$ for arbitrary $\mathbf{k}\in\{\mathbf{k}\}_{\in\mathrm{BZ}}\backslash(\mathrm{K}\vee\bar{\mathrm{K}})$. This EWF zero distribution is consistent with a constraint $C_{\mathrm{exc}}=\pm 2 \bmod 6$ in C_6 symmetric systems [60].

Exciton condensation and f-wave spin-split magnons—Next, we discuss how the topological excitons behave in the vicinity of the phase boundary between the paramagnetic and magnetic phases. Figure 2(b) shows the excitation spectrum when $(t_2,U)/t_1=(0.215,4)$, which is very close to the phase boundary yet still in the paramagnetic phase. The topological excitons are ready to condense at the Γ point. Their condensation at $(t_2,U)/t_1\approx(0.212,4)$ drives the onset of Néel antiferromagnetic order indicated in Fig. 1(d) and the phase transition into the topological AFM phase B. It is also worth noting that, as indicated in Fig. 1(c), the exciton condensation obtained with the TDHF almost perfectly coincides with the nonmagnetic-magnetic phase boundary obtained with HF, suggesting that the mean-field transition can be understood in terms of topological exciton condensation.

Upon exciton condensation, the resulting magnetically ordered state supports magnon excitations that continuously evolve from the excitonic modes of the paramagnetic phase and exhibit linearly dispersive Type-I Goldstone-mode behavior. Remarkably, the gapless magnon modes of the odd-parity magnetic state display f-wave spin splitting, as indicated in Figs. 2(c) and 2(d) and its inset. The dispersion relations of magnons with upward and downward spin-flip processes are nondegenerate at general wave numbers and are connected by $\omega_{\mathbf{q},\pm\mp}=C_{3\parallel}^{\pm 1}\omega_{-\mathbf{q},\mp\pm}$, where $C_{3\parallel}$ denotes threefold rotation around the out-of-plane axis. Note that the long-wavelength behavior of the odd-parity magnons as Type-I Goldstone modes is ensured by the spontaneous breaking of the spin-space SO(3) symmetry into SO(2). Our calculation presents the first identification of nonrelativistic collinear odd-parity magnons in an itinerant model. Note that the f-wave magnon spin splitting is associated with those of electron bands induced by loop currents [34,35,61], where spin-space $C_{2\perp}\mathcal{T}$ is broken while spin-space $C_{2\perp}$ followed by real-space inversion $\mathscr{P}$ is preserved. The Chern numbers of spin-split magnons are -2 for both upward and downward spin flips, as shown in Figs. 2(c) and 2(d), indicating that Eq. (9) connecting exciton and electron Chern numbers remains valid even in the topological odd-parity AFM phase B. Importantly, the quasiparticle Chern numbers are necessarily preserved across the exciton-condensation transition, despite the evolution from gapped excitons to gapless Goldstone magnons. This topological continuity follows from Sylvester's law of inertia for bosonic BdG systems [62].

Magnon bandgap closing enforced by electron bandgap closing—We next discuss the transition from a topological to a nontopological AFM phase. It is long known that the

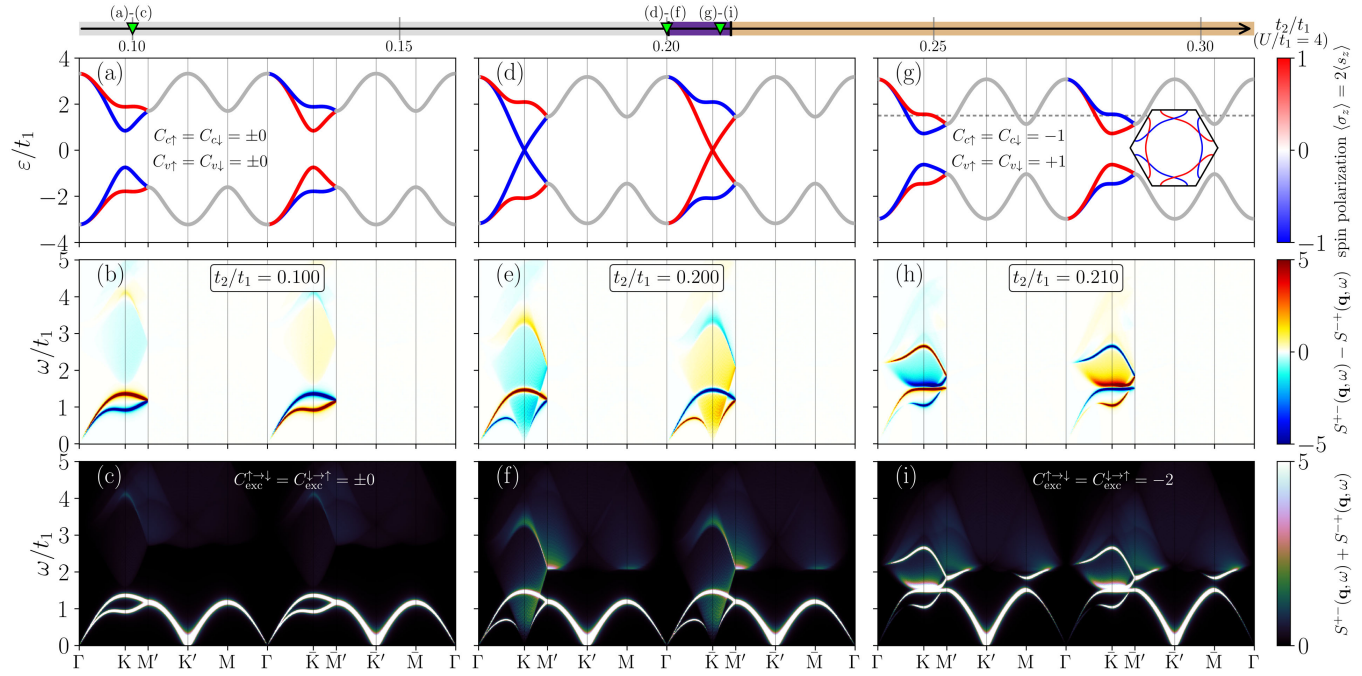


FIG. 4. (a),(d),(g) Electron bands near the nontopological-topological AFM phase boundary obtained with Hartree-Fock approximation. Red, blue, and gray bands indicate up-spin, down-spin, and spin-degenerate ones, respectively. Inset [in (g)]: the isoenergy contour of the electron bands at $\varepsilon/t_1 = 1.5$, corresponding to the gray dashed line. (b),(e),(h) Difference in spin-resolved dynamical spin-structure factors $S_{+-}(\mathbf{q},\omega) - S_{-+}(\mathbf{q},\omega)$. (c),(f),(i) Dynamical spin-structure factor $S(\mathbf{q},\omega) = S_{+-}(\mathbf{q},\omega) + S_{-+}(\mathbf{q},\omega)$. For all panels, $U/t_1 = 4$ and $\phi = \pi/2$. The value of t_2/t_1 is common to each column and is indicated in the corresponding panels as well as marked in the phase diagram at the top. Light gray, purple, and orange bands in the phase diagram show phases C, B, and A, respectively.

phase transition originates from the gap closing and reopening of the f-wave spin-split electron bands [14,61] at K and $\bar{\mathrm{K}}$ points, which is reproduced in Figs. 4(a), 4(d), and 4(g). This gap closing induces a downward shift of the spin-resolved particle-hole continuum toward low energy at K and $\bar{\mathrm{K}}$ points, as clearly seen in Figs. 4(c), 4(f), and 4(i). In particular, when the electron bandgap closes for $(t_2, U)/t_1 \approx (0.200, 4)$, the continuum touches zero energy, as shown in Fig. 4(f). Since f-wave spin-split magnons are excitonic particle-hole bound states, thus always lower in energy than the particle-hole continuum, it is ensured that such magnons touch the upper continua. This *enforced* magnon bandgap closing leads to a change in magnon topology from $C_{\rm exc}^{\bar{\sigma}\to\sigma} = -2$ to $C_{\rm exc}^{\bar{\sigma}\to\sigma} = \pm 0$, highlighting nontrivial correlation between magnons as particle-hole bound states and the upper particle-hole continua [63]. This also ensures the validity of Eq. (9) even in the nontopological AFM phase C.

It is also worth pointing out that, within the topological odd-parity AFM phase B, spin-split magnons exhibit *avoided decaylike* features [64,65] near K and $\bar{\mathrm{K}}$ points, in which bound states are pushed out of the continuum by strong interaction effects, as seen in Figs. 4(e) and 4(h). As a result, the magnitude of f-wave magnon spin splitting is drastically enhanced. Note that a similar enhanced spin splitting by the avoided decaylike mechanism has recently been reported for even-parity altermagnets near the metal-insulator transition [66].

Discussion—Our results establish a continuous evolution of topological collective excitations across the onset of magnetic order in the Haldane-Hubbard model. Topological excitons of the paramagnetic phase condense to form the collinear Néel state and continuously evolve into f-wave spin-split gapless magnons. The connection extends to topological transitions within the ordered phase, where an electronic bandgap closing enforces a magnon bandgap closing and changes the topology of the collective modes. Our work provides the first realization of nonrelativistic odd-parity magnons in a collinear itinerant system and, more broadly, demonstrates how topology and unconventional magnetic symmetry can be carried across phase transitions driven by collective excitations. The itinerant nature of these excitations further allows their spin splitting to be strongly enhanced through coupling to the particle-hole continuum, highlighting physics beyond localized-spin descriptions.

These phenomena provide several routes toward experimental realization. Floquet-engineered collinear antiferromagnets [61,67–73] offer a natural setting in which odd-parity spin splitting can appear in both electronic and collective magnetic excitations. While photodrive-induced heating generally limits Floquet realizations, in the high-frequency regime a prethermal window can provide a long

but finite timescale over which an effective Floquet Hamiltonian and its collective excitations remain well defined [44,74–77]. Alternatively, ultrashort driving protocols may access transient Floquet-engineered states on subcycle timescales before dissipative processes become dominant, as demonstrated experimentally for Floquet-Bloch bands [78]. For the magnetically ordered regime, thermal fluctuations provide an additional consideration. In the strictly two-dimensional spin-rotation-symmetric limit, finite-temperature long-range Néel order is excluded by the Mermin-Wagner theorem [79,80], while weak easy-axis magnetic anisotropy or interlayer coupling can stabilize the ordered phase in solid-state realizations. Such anisotropy is absent in Eq. (1) and may arise from weak spin-orbit coupling, for example, due to substrate or proximity effects. Importantly, the excitonic side of this physics does not require long-range magnetic order: topological exciton modes should already be present in the paramagnetic regime, suggesting Floquet-engineered paramagnets such as graphene [81–85] as another possible platform.

Cold-atom realizations provide a complementary route since the noninteracting Haldane model has already been implemented in optical lattices [86,87]. Probing the momentum-resolved collective excitation spectrum could directly reveal the predicted evolution from topological excitons to odd-parity spin-split magnons [88].

Note added—Recently, we became aware of Ref. [89], which studies Floquet nonrelativistic odd-parity magnons using an effective spin model.

Acknowledgments—We thank Henry Davenport for helpful feedback on the manuscript. R. E. thanks Alexander Mook for pointing out Ref. [54]. J. K. thanks Valentin Leeb for discussion and related collaborations. We acknowledge support from the Deutsche Forschungsgemeinschaft (DFG, German Research Foundation) under Germany's Excellence Strategy (EXC–2111–390814868 and ct.qmat EXC-2147-390858490) and DFG Grants No. KN1254/1-2, No. KN1254/2-1 TRR 360–492547816, and No. SFB 1143 (Project No. 247310070), as well as the Munich Quantum Valley, which is supported by the Bavarian state government with funds from the Hightech Agenda Bayern Plus. J. K. thanks the Keck foundation for support. R. E. acknowledges financial support by JSPS Overseas Fellowship.

Data availability—Simulation codes are available on Zenodo [90].

[1] F. Wu, T. Lovorn, and A. H. MacDonald, Topological exciton bands in moiré heterojunctions, Phys. Rev. Lett. **118**, 147401 (2017).
[2] K. Chen and R. Shindou, Chiral topological excitons in a Chern band insulator, Phys. Rev. B **96**, 161101(R) (2017).
[3] Y. H. Kwan, Y. Hu, S. H. Simon, and S. A. Parameswaran, Exciton band topology in spontaneous quantum anomalous Hall insulators: Applications to twisted bilayer graphene, Phys. Rev. Lett. **126**, 137601 (2021).
[4] H. Zheng, K. Yang, T. Cao, and D. Xiao, Topological charge-transfer excitons, arXiv:2608.05308.
[5] Y. Hwang, H. Davenport, and F. Schindler, Exciton alchemy: Chern excitons from trivial bands, arXiv:2608.07372.
[6] P. A. McClarty, Topological magnons: A review, Annu. Rev. Condens. Matter Phys. **13**, 171 (2022).
[7] T. Zhang, Y. Liu, H. Miao, and S. Murakami, Advances in phonons: From band topology to phonon chirality, arXiv:2505.06179.
[8] F. D. M. Haldane, Model for a quantum Hall effect without Landau levels: Condensed-matter realization of the "parity anomaly," Phys. Rev. Lett. **61**, 2015 (1988).
[9] C. L. Kane and E. J. Mele, Z_2 topological order and the quantum spin Hall effect, Phys. Rev. Lett. **95**, 146802 (2005).
[10] C. L. Kane and E. J. Mele, Quantum spin Hall effect in graphene, Phys. Rev. Lett. **95**, 226801 (2005).
[11] S. Rachel and K. Le Hur, Topological insulators and mott physics from the Hubbard interaction, Phys. Rev. B **82**, 075106 (2010).
[12] T. Neupert, L. Santos, C. Chamon, and C. Mudry, Fractional quantum Hall states at zero magnetic field, Phys. Rev. Lett. **106**, 236804 (2011).
[13] S. Rachel, Interacting topological insulators: A review, Rep. Prog. Phys. **81**, 116501 (2018).
[14] V. S. Arun, R. Sohal, C. Hickey, and A. Paramekanti, Mean field study of the topological Haldane-Hubbard model of spin-$\frac{1}{2}$ fermions, Phys. Rev. B **93**, 115110 (2016).
[15] C. Hickey, L. Cincio, Z. Papić, and A. Paramekanti, Haldane-Hubbard mott insulator: From tetrahedral spin crystal to chiral spin liquid, Phys. Rev. Lett. **116**, 137202 (2016).
[16] T. I. Vanhala, T. Siro, L. Liang, M. Troyer, A. Harju, and P. Törmä, Topological phase transitions in the repulsively interacting Haldane-Hubbard model, Phys. Rev. Lett. **116**, 225305 (2016).
[17] E. Alba, J. K. Pachos, and J. J. García-Ripoll, Winding number order in the Haldane model with interactions, New J. Phys. **18**, 033022 (2016).
[18] L. S. G. Leite and R. L. Doretto, Flat-band ferromagnetism and spin waves in the Haldane-Hubbard model, Phys. Rev. B **104**, 155129 (2021).
[19] T.-C. Yi, H.-Q. Lin, and R. Mondaini, Higher-order topological insulator in a modified Haldane-Hubbard model, Phys. Rev. B **107**, 165135 (2023).
[20] B.-Q. Wang, C. Shao, T. Tohyama, H.-G. Luo, and H. Lu, Topological phase in the extended Haldane-Hubbard model with sublattice-dependent repulsion, Phys. Rev. B **110**, 035107 (2024).
[21] W.-X. He, R. Mondaini, H.-G. Luo, X. Wang, and S. Hu, Phase transitions in the Haldane-Hubbard model, Phys. Rev. B **109**, 035126 (2024).
[22] Z.-L. Gu, Z.-Y. Dong, S.-L. Yu, and J.-X. Li, Itinerant topological magnons in Haldane Hubbard model with a nearly-flat electron band, arXiv:1908.09255.
[23] L. Šmejkal, J. Sinova, and T. Jungwirth, Beyond conventional ferromagnetism and antiferromagnetism: A phase

with nonrelativistic spin and crystal rotation symmetry, Phys. Rev. X **12**, 031042 (2022).
[24] L. Šmejkal, J. Sinova, and T. Jungwirth, Emerging research landscape of altermagnetism, Phys. Rev. X **12**, 040501 (2022).
[25] I. Mazin (The PRX Editors), Editorial: Altermagnetism—a new punch line of fundamental magnetism, Phys. Rev. X **12**, 040002 (2022).
[26] A. B. Hellenes, T. Jungwirth, R. Jaeschke-Ubiergo, A. Chakraborty, J. Sinova, and L. Šmejkal, P-wave magnets, arXiv:2309.01607.
[27] B. Brekke, P. Sukhachov, H. G. Giil, A. Brataas, and J. Linder, Minimal models and transport properties of unconventional p-wave magnets, Phys. Rev. Lett. **133**, 236703 (2024).
[28] Y. Yu, M. B. Lyngby, T. Shishidou, M. Roig, A. Kreisel, M. Weinert, B. M. Andersen, and D. F. Agterberg, Odd-parity magnetism driven by antiferromagnetic exchange, Phys. Rev. Lett. **135**, 046701 (2025).
[29] N. A. A. Pari, R. Jaeschke-Ubiergo, A. Chakraborty, L. Šmejkal, and J. Sinova, Nonrelativistic linear edelstein effect in helical $euin_2as_2$, Phys. Rev. B **112**, 024404 (2025).
[30] A. Chakraborty, A. Birk Hellenes, R. Jaeschke-Ubiergo, T. Jungwirth, L. Šmejkal, and J. Sinova, Highly efficient nonrelativistic Edelstein effect in nodal p-wave magnets, Nat. Commun. **16**, 7270 (2025).
[31] Q. Song, S. Stavrić, P. Barone, A. Droghetti, D. S. Antonenko, J. W. F. Venderbos, C. A. Occhialini, B. Ilyas, E. Ergeçen, N. Gedik, S.-W. Cheong, R. M. Fernandes, S. Picozzi, and R. Comin, Electrical switching of a p-wave magnet, Nature (London) **642**, 64 (2025).
[32] R. Yamada *et al.*, A metallic p-wave magnet with commensurate spin helix, Nature (London) **646**, 837 (2025).
[33] T. Sato, S. Haddad, I. C. Fulga, F. F. Assaad, and J. van den Brink, Altermagnetic anomalous Hall effect emerging from electronic correlations, Phys. Rev. Lett. **133**, 086503 (2024).
[34] V. Leeb and J. Knolle, Collinear p-wave magnetism and hidden orbital ferrimagnetism, Phys. Rev. Lett. **137**, 106701 (2026).
[35] Y.-P. Lin and M. Vila, Odd-parity altermagnetism through sublattice currents: From Haldane-Hubbard model to general bipartite lattices, Phys. Rev. Lett. **137**, 066702 (2026).
[36] T. A. Maier and S. Okamoto, Weak-coupling theory of neutron scattering as a probe of altermagnetism, Phys. Rev. B **108**, L100402 (2023).
[37] L. Šmejkal, A. Marmodoro, K.-H. Ahn, R. González-Hernández, I. Turek, S. Mankovsky, H. Ebert, S. W. D'Souza, O. c. v. Šipr, J. Sinova, and T. c. v. Jungwirth, Chiral magnons in altermagnetic ruo_2, Phys. Rev. Lett. **131**, 256703 (2023).
[38] A. T. Costa, J. C. G. Henriques, and J. Fernández-Rossier, Giant spatial anisotropy of magnon Landau damping in altermagnets, SciPost Phys. **18**, 125 (2025).
[39] F. Garcia-Gaitan, A. Kefayati, J. Q. Xiao, and B. K. Nikolić, Magnon spectrum of altermagnets beyond linear spin wave theory: Magnon-magnon interactions via time-dependent matrix product states versus atomistic spin dynamics, Phys. Rev. B **111**, L020407 (2025).
[40] Y. Liu, S. Shao, S. He, Z. Y. Xie, J.-W. Mei, H.-G. Luo, and J. Zhao, Quantum dynamics in a spin-$\frac{1}{2}$ square lattice $J_1 - J_2 - \delta$ altermagnet, Phys. Rev. B **111**, 245117 (2025).
[41] R. Eto, M. Gohlke, J. Sinova, M. Mochizuki, A. L. Chernyshev, and A. Mook, Spontaneous magnon decays from nonrelativistic time-reversal symmetry breaking in altermagnets, Phys. Rev. B **112**, 094442 (2025).
[42] R. R. Neumann, R. Jaeschke-Ubiergo, R. Zarzuela, L. Šmejkal, J. Sinova, and A. Mook, Odd-parity-wave magnons and nonrelativistic thermal Edelstein effect, arXiv:2603.05415.
[43] V. P. Kravchuk, K. V. Yershov, B. Pradenas, R. R. Neumann, R. Jaeschke-Ubiergo, R. Zarzuela, J. Sinova, J. van den Brink, and A. Mook, Nonlinear magnon magnetic moment transport in triangular-lattice f-wave antialtermagnets, Phys. Rev. B **114**, 194410 (2026).
[44] N. Goldman and J. Dalibard, Periodically driven quantum systems: Effective Hamiltonians and engineered gauge fields, Phys. Rev. X **4**, 031027 (2014).
[45] D. Thouless, Stability conditions and nuclear rotations in the Hartree-Fock theory, Nucl. Phys. **21**, 225 (1960).
[46] D. Thouless, Vibrational states of nuclei in the random phase approximation, Nucl. Phys. **22**, 78 (1961).
[47] A. D. McLachlan and M. A. Ball, Time-dependent Hartree—Fock theory for molecules, Rev. Mod. Phys. **36**, 844 (1964).
[48] J. W. Negele, The mean-field theory of nuclear structure and dynamics, Rev. Mod. Phys. **54**, 913 (1982).
[49] M. Nalabothula, D. Sangalli, F. Paleari, S. Reichardt, and L. Wirtz, Symmetries of excitons, Phys. Rev. B **113**, 205130 (2026).
[50] T. Tan, P. J. Ledwith, and T. Devakul, The ideal limit of rhombohedral graphene: Interaction-induced layer-skyrmion lattices and their collective excitations, arXiv:2511.07402.
[51] M. R. Hirsbrunner, F. Desrochers, J. Huxford, and Y. B. Kim, Topological phonons in anomalous Hall crystals, arXiv:2601.06246.
[52] H. Davenport, J. Knolle, and F. Schindler, Exciton berryology, Phys. Rev. B **113**, 045125 (2026).
[53] H. Davenport, F. Schindler, and J. Knolle, Berry curvature of low-energy excitons in rhombohedral graphene, Phys. Rev. B **113**, 115102 (2026).
[54] W.-T. Zhou, Z.-Y. Dong, Z.-L. Gu, and J.-X. Li, Itinerant topological magnons and spin excitons in twisted transition metal dichalcogenides: Mapping electron topology to its spin counterpart, Natl. Sci. Rev. **13**, nwaf354 (2026).
[55] J. Colpa, Diagonalization of the quadratic boson Hamiltonian, Physica A (Amsterdam) **93**, 327 (1978).
[56] T. Fukui, Y. Hatsugai, and H. Suzuki, Chern numbers in discretized brillouin zone: Efficient method of computing (spin) Hall conductances, J. Phys. Soc. Jpn. **74**, 1674 (2005).
[57] T. Olsen, Unified treatment of magnons and excitons in monolayer cri_3 from many-body perturbation theory, Phys. Rev. Lett. **127**, 166402 (2021).
[58] H.-Y. Xie, P. Ghaemi, M. Mitrano, and B. Uchoa, Theory of topological exciton insulators and condensates in flat Chern bands, Proc. Natl. Acad. Sci. U.S.A. **121**, e2401644121 (2024).
[59] H. Davenport, J. Knolle, and F. Schindler, Interaction-induced crystalline topology of excitons, Phys. Rev. Lett. **133**, 176601 (2024).
[60] Y. Hwang, H. Davenport, and F. Schindler, Stable wavefunction zeros indicate exciton topology, arXiv:2604.21643.

[61] T. Zhu, D. Zhou, H. Wang, S.-H. Wei, and J. Ruan, Floquet odd-parity collinear magnets, Phys. Rev. Lett. **136**, 126704 (2026).
[62] R. Shindou, R. Matsumoto, S. Murakami, and J.-i. Ohe, Topological chiral magnonic edge mode in a magnonic crystal, Phys. Rev. B **87**, 174427 (2013).
[63] X. Cai, A. Consiglio, D. Di Sante, R. Thomale, and W. Hanke, Continuum theory for topological phase transitions in exciton systems, Phys. Rev. B **113**, 205121 (2026).
[64] R. Verresen, R. Moessner, and F. Pollmann, Avoided quasiparticle decay from strong quantum interactions, Nat. Phys. **15**, 750 (2019).
[65] X. Wang, R. Moessner, and D. Chowdhury, Interaction-mitigated Landau damping, Phys. Rev. B **109**, L121102 (2024).
[66] J. Issing, M. Dürrnagel, S. Mazumdar, A. Lorenz, N. Witt, G. Sangiovanni, M. Klett, L. Klebl, R. Thomale, and J. Seufert, Altermagnons at the metal-insulator transition, arXiv:2605.11669.
[67] S. A. A. Ghorashi and Q. Li, Dynamical generation of higher-order spin-orbit coupling, topology, and persistent spin texture in light-irradiated altermagnets, Phys. Rev. Lett. **135**, 236702 (2025).
[68] P.-H. Fu, S. Mondal, J.-F. Liu, Y. Tanaka, and J. Cayao, Floquet engineering spin triplet states in unconventional magnets, Phys. Rev. Lett. **136**, 066703 (2026).
[69] S. Huang, Z. Qin, F. Zhan, D.-H. Xu, D.-S. Ma, and R. Wang, Light-induced odd-parity magnetism in conventional antiferromagnetism, Phys. Rev. Lett. **136**, 126703 (2026).
[70] B. Li, D.-F. Shao, and A. A. Kovalev, Floquet spin splitting and spin generation in antiferromagnets, Phys. Rev. Lett. **136**, 166701 (2026).
[71] T. Zhang, Z. Xiao, T. Fang, and Z. Wang, Light-induced switchable odd-parity altermagnetism in one- and two-dimensional triangulene crystals, Nano Lett. **26**, 4889 (2026).
[72] D. Liu, Z.-Y. Zhuang, D. Zhu, Z. Wu, and Z. Yan, Light-induced odd-parity altermagnets on dimerized lattices, Phys. Rev. B **113**, L060409 (2026).
[73] Y. Tian, C.-H. Zhao, C.-B. Wang, B. Zhang, X. Kong, and W.-J. Gong, Optically driven orbital Hall transport in Floquet odd-parity collinear altermagnets with high Chern numbers, arXiv:2603.11483.
[74] D. A. Abanin, W. De Roeck, and F. m. c. Huveneers, Exponentially slow heating in periodically driven many-body systems, Phys. Rev. Lett. **115**, 256803 (2015).
[75] T. Mori, T. Kuwahara, and K. Saito, Rigorous bound on energy absorption and generic relaxation in periodically driven quantum systems, Phys. Rev. Lett. **116**, 120401 (2016).
[76] T. Kuwahara, T. Mori, and K. Saito, Floquet–Magnus theory and generic transient dynamics in periodically driven many-body quantum systems, Ann. Phys. (Amsterdam) **367**, 96 (2016).
[77] D. A. Abanin, W. De Roeck, W. W. Ho, and F. m. c. Huveneers, Effective Hamiltonians, prethermalization, and slow energy absorption in periodically driven many-body systems, Phys. Rev. B **95**, 014112 (2017).
[78] S. Ito, M. Schüler, M. Meierhofer, S. Schlauderer, J. Freudenstein, J. Reimann, D. Afanasiev, K. A. Kokh, O. E. Tereshchenko, J. Güdde, M. A. Sentef, U. Höfer, and R. Huber, Build-up and dephasing of Floquet–Bloch bands on subcycle timescales, Nature (London) **616**, 696 (2023).
[79] N. D. Mermin and H. Wagner, Absence of ferromagnetism or antiferromagnetism in one- or two-dimensional isotropic Heisenberg models, Phys. Rev. Lett. **17**, 1133 (1966).
[80] P. Bruno, Absence of spontaneous magnetic order at nonzero temperature in one- and two-dimensional Heisenberg and *XY* systems with long-range interactions, Phys. Rev. Lett. **87**, 137203 (2001).
[81] T. Oka and H. Aoki, Photovoltaic Hall effect in graphene, Phys. Rev. B **79**, 081406(R) (2009).
[82] M. A. Sentef, M. Claassen, A. F. Kemper, B. Moritz, T. Oka, J. K. Freericks, and T. P. Devereaux, Theory of Floquet band formation and local pseudospin textures in pump-probe photoemission of graphene, Nat. Commun. **6**, 7047 (2015).
[83] M. Schüler, U. De Giovannini, H. Hübener, A. Rubio, M. A. Sentef, T. P. Devereaux, and P. Werner, How circular dichroism in time- and angle-resolved photoemission can be used to spectroscopically detect transient topological states in graphene, Phys. Rev. X **10**, 041013 (2020).
[84] M. Merboldt, M. Schüler, D. Schmitt, J. P. Bange, W. Bennecke, K. Gadge, K. Pierz, H. W. Schumacher, D. Momeni, D. Steil, S. R. Manmana, M. A. Sentef, M. Reutzel, and S. Mathias, Observation of Floquet states in graphene, Nat. Phys. **21**, 1093 (2025).
[85] M. A. Sentef and M. Reutzel, A Floquet gap finally opens in graphene, Nat. Mater. **25**, 1080 (2026).
[86] G. Jotzu, M. Messer, R. Desbuquois, M. Lebrat, T. Uehlinger, D. Greif, and T. Esslinger, Experimental realization of the topological Haldane model with ultracold fermions, Nature (London) **515**, 237 (2014).
[87] M. Aidelsburger, M. Lohse, C. Schweizer, M. Atala, J. T. Barreiro, S. Nascimbène, N. R. Cooper, I. Bloch, and N. Goldman, Measuring the Chern number of Hofstadter bands with ultracold bosonic atoms, Nat. Phys. **11**, 162 (2015).
[88] P. T. Ernst, S. Götze, J. S. Krauser, K. Pyka, D.-S. Lühmann, D. Pfannkuche, and K. Sengstock, Probing superfluids in optical lattices by momentum-resolved bragg spectroscopy, Nat. Phys. **6**, 56 (2010).
[89] P. Zhang, S.-B. Xie, J. Yu, Y. Liu, and C.-C. Liu, Odd-parity magnons, arXiv:2605.31411.
[90] R. Eto, Odd-parity magnons in the Haldane-Hubbard model from topological exciton condensation [dataset], https://doi.org/10.5281/zenodo.23664459.
[91] J. R. Schrieffer, X.-G. Wen, and S.-C. Zhang, Spin-bag mechanism of high-temperature superconductivity, Phys. Rev. Lett. **60**, 944 (1988).
[92] J. R. Schrieffer, X. G. Wen, and S. C. Zhang, Dynamic spin fluctuations and the bag mechanism of high-T_c superconductivity, Phys. Rev. B **39**, 11663 (1989).
[93] J. Knolle, I. Eremin, A. V. Chubukov, and R. Moessner, Theory of itinerant magnetic excitations in the spin-density-wave phase of iron-based superconductors, Phys. Rev. B **81**, 140506(R) (2010).

[94] J. Knolle, I. Eremin, and R. Moessner, Multiorbital spin susceptibility in a magnetically ordered state: Orbital versus excitonic spin density wave scenario, Phys. Rev. B **83**, 224503 (2011).

[95] J. Willsher, H.-K. Jin, and J. Knolle, Magnetic excitations, phase diagram, and order-by-disorder in the extended triangular-lattice Hubbard model, Phys. Rev. B **107**, 064425 (2023).

End Matter

Appendix A: Hartree-Fock—In the Hartree-Fock approximation, we decompose the onsite Hubbard interaction in Eq. (1) as follows:

$$\hat{n}_{\mathbf{r}\uparrow}\hat{n}_{\mathbf{r}\downarrow} \approx \langle \hat{n}_{\mathbf{r}\uparrow}\rangle \hat{n}_{\mathbf{r}\downarrow} + \hat{n}_{\mathbf{r}\uparrow}\langle \hat{n}_{\mathbf{r}\downarrow}\rangle - \langle \hat{n}_{\mathbf{r}\uparrow}\rangle\langle \hat{n}_{\mathbf{r}\downarrow}\rangle. \tag{A1}$$

Note that, since we are now interested only in paramagnetic and collinear orders, we practically omit the Fock terms with spin flip in our calculation. Indeed, in the parameter region shown in Fig. 1(c), noncollinear and noncoplanar orders are not the mean-field ground state [14].

Within the Hartree-Fock approximation, electron bands and Bloch states are obtained with the following momentum-resolved eigenvalue problem:

$$\hat{H}^{\mathrm{MF}}_{\sigma}(\mathbf{k})\left|\mathbf{k}, v/c\sigma\right\rangle = \varepsilon_{\mathbf{k},v/c\sigma}\left|\mathbf{k}, v/c\sigma\right\rangle, \tag{A2}$$

where

$$\hat{H}^{\mathrm{MF}}_{\sigma}(\mathbf{k}) = \hat{\mathbf{c}}^{\dagger}_{\sigma}\begin{pmatrix} +\iota(\mathbf{k}) + U\langle \hat{n}_{\mathrm{A}\bar{\sigma}}\rangle & \gamma(\mathbf{k}) \\ \gamma^{*}(\mathbf{k}) & -\iota(\mathbf{k}) + U\langle \hat{n}_{\mathrm{B}\bar{\sigma}}\rangle \end{pmatrix}\hat{\mathbf{c}}_{\sigma}. \tag{A3}$$

Now $\hat{\mathbf{c}}^{\dagger}_{\sigma} = (\hat{c}^{\dagger}_{\mathbf{k},\mathrm{A}\sigma}, \hat{c}^{\dagger}_{\mathbf{k},\mathrm{B}\sigma})$ and

$$\iota(\mathbf{k}) = -2t_2\sum_{i=1,2,3}\cos(\mathbf{k}\cdot\mathbf{a}_i + \phi),$$
$$\gamma(\mathbf{k}) = -t_1(1 + e^{\mathrm{i}\mathbf{k}\cdot\mathbf{a}_3} + e^{-\mathrm{i}\mathbf{k}\cdot\mathbf{a}_2}). \tag{A4}$$

A and B are sublattice indices.

Appendix B: Random-phase approximation—Within the RPA, spin-resolved dynamical structure factors are obtained from the RPA susceptibility tensor as

$$S_{\pm\mp}(\mathbf{q},\omega) = -\frac{1}{\pi}\sum_{\alpha\beta}\mathrm{Im}\{[\chi^{\mathrm{RPA}}_{\pm\mp}(\mathbf{q},\omega + \mathrm{i}0^{+})]_{\alpha\beta}e^{-\mathrm{i}\mathbf{q}\cdot(\boldsymbol{\delta}_{\alpha}-\boldsymbol{\delta}_{\beta})}\}, \tag{B1}$$

where $\boldsymbol{\delta}_{\mathrm{A}} = (0,0)$ and $\boldsymbol{\delta}_{\mathrm{B}} = (0, 1/\sqrt{3})$ denote internal coordinates of sublattices within a unit cell. 0^{+} denotes an infinitesimal positive number. The RPA susceptibility tensor is obtained by resumming the bare susceptibility tensor as

$$\chi^{\mathrm{RPA}}_{\pm\mp}(\mathbf{q},\mathrm{i}\omega_n) = \frac{\chi^{0}_{\pm\mp}(\mathbf{q},\mathrm{i}\omega_n)}{1 - U\chi^{0}_{\pm\mp}(\mathbf{q},\mathrm{i}\omega_n)}, \tag{B2}$$

where 1 denotes an identity. This formula is valid for arbitrary onsite Hubbard models with spin-σ_z conservation, and the HH model given by Eq. (1) falls into this category. The explicit form of the bare susceptibility tensor χ^{0} is constructed from the Hartree-Fock eigenenergies and eigenstates [91–95] as

$$[\chi^{0}_{\pm\mp}(\mathbf{q},\mathrm{i}\omega_n)]_{\alpha\beta} = -\frac{1}{N_{\mathbf{k}}}\sum_{\mathbf{k}}\sum_{\nu_1,\nu_2}\frac{f(\varepsilon_{\mathbf{k},\nu_1}-\mu) - f(\varepsilon_{\mathbf{k}+\mathbf{q},\nu_2}-\mu)}{\mathrm{i}\omega_n + \varepsilon_{\mathbf{k},\nu_1} - \varepsilon_{\mathbf{k}+\mathbf{q},\nu_2}} \times \langle \mathbf{k},\nu_1|\sigma^{\pm}_{\alpha}|\mathbf{k}+\mathbf{q},\nu_2\rangle\langle \mathbf{k}+\mathbf{q},\nu_2|\sigma^{\mp}_{\beta}|\mathbf{k},\nu_1\rangle, \tag{B3}$$

where $\omega_n = 2n\pi k_{\mathrm{B}}T\,(n\in\mathbb{Z})$ denotes the bosonic Matsubara frequency. $f(\varepsilon) = [\exp(\varepsilon/k_{\mathrm{B}}T)+1]^{-1}$ denotes the Fermi-Dirac distribution function. μ is chemical potential.